Polymer Chemistry

PAPER

View Article Online
View Journal | View Issue

Check for updates

Cite this: *Polym. Chem.*, 2019, **10**, 1442

Vat photopolymerization of charged monomers: 3D printing with supramolecular interactions†

Emily M. Wilts,[a] Allison M. Pekkanen,[b] B. Tyler White, [a]
Viswanath Meenakshisundaram,[c] Donald C. Aduba Jr.,[c] Christopher B. Williams[c] and
Timothy E. Long *[a]

Received 18th December 2018,
Accepted 31st January 2019

DOI: 10.1039/c8py01792a

rsc.li/polymers

Additive manufacturing enables the creation of novel structures and geometries previously unattainable through traditional processing techniques. In particular, vat photopolymerization provides unprecedented resolution through the tailored delivery of light with photo-crosslinkable or photo-polymerizable materials. Traditionally, chemical crosslinks generate a permanent network, which exhibits swelling but not dissolution. In this work, photopolymerization of photo-reactive monomers with acrylate, acrylamide, and vinyl polymerizable sites enabled the formation of water-soluble 3D printed parts using vat photopolymerization. A library of monomers with varied ionic and hydrogen bonding sites provided photopolymerized films with tensile properties approaching 1200% elongation at break and 0.47 MPa stress at 100% elongation. The rate of polymerization and the subsequent mechanical properties revealed a dependence on the type of supramolecular interactions and functionality on the resulting hydrogel. The diverse functionality of the monomers enabled aqueous dissolution times ranging from 27 to 41 min. Vat photopolymerization of a trimethylammonium ethyl acrylate chloride solution and with 30 wt% *N*-vinyl pyrrolidone provided 3D parts with fine structural resolution. This method of creating soluble, water-swollen structures through vat photopolymerization provides future research with a larger library of monomers for diverse applications including soluble support scaffolds.

1. Introduction

Additive manufacturing (AM) provides a unique method for the creation of complex geometries, which enables the design of features that enable enhanced functionality.[1,2] Many AM processes currently exist, including material extrusion, powder-bed fusion, and vat photopolymerization.[3,4] These methods enable the control of geometry and porosity throughout the resulting part, reduction of waste compared to traditional manufacturing, and design of previously unattainable geometries.[5] Vat photopolymerization, also referred to as stereolithography, operates through the selective patterning of UV light with vats of photopolymer precursors containing photoinitiator to create chemically or physically crosslinked solids.[4] Upon the introduction of light, chemical crosslinking occurs at the site of irradiation to form a solid network with a characteristic depth, which depends on light intensity, exposure time, photoinitiator content, and presence of photoabsorbers.[6,7] Advantages of vat photopolymerization relative to other printing technologies include fabricating micron-scale features, excellent surface finish, and accuracy of printed parts.[8,9] However, a limited material selection restricts vat photopolymerization as traditional processes typically require a low viscosity, photo-crosslinkable oligomeric precursor that leads to chemical crosslinking to successfully form 3D parts.[10]

Supramolecular interactions employ reversible, non-covalent bonding between molecules and polymers. Commonly investigated supramolecular interactions in polymers include ionic interactions, hydrogen bonding, metal–ligand coordination, and pi–pi stacking.[11] Ionic interactions and hydrogen bonding continue to play a critical role in the creation of complex structures through ionic aggregation and multiple hydrogen bonding motifs.[12,13] While typically weaker than covalent bonds, the synergistic effect of collective interactions significantly enhances the intermolecular forces between polymer chains.[12] Supramolecular interactions offer impact in adhesive and biomedical applications due to their reversibility under stimuli and the breadth of interactions found in nature.[12,14–16] Additionally, the ability of supramolecular interactions to

---

[a] Department of Chemistry, Macromolecules Innovation Institute, Virginia Tech, Blacksburg, VA 24061, USA. E-mail: telong@vt.edu; Fax: +(540) 231-8517; Tel: +(540) 231-2480

[b] School of Biomedical Engineering and Sciences, Virginia Tech, Blacksburg, VA 24061, USA

[c] Department of Mechanical Engineering, Virginia Tech, Blacksburg, VA 24061, USA

† Electronic supplementary information (ESI) available. See DOI: 10.1039/c8py01792a

reduce or eliminate anisotropic strength profiles in AM parts remains a focus of recent research.[17] Liska *et al.* detailed the examination of monofunctional monomers for vat photopolymerization, but failed to realize well-defined parts without incorporation of chemical crosslinkers.[18] The ability to probe supramolecular interactions to form well-defined 3D networks without the need for chemical crosslinking remains unexplored.

The generation of complex additively manufactured parts also often requires support scaffolds to hold over-hanging structures in place during printing. Because vat photopolymerization traditionally utilizes permanent, covalent crosslinks, dissolvable support scaffolds fail to exist. Current methods to produce sacrificial support structures rely on digital grayscale images, which produce partially crosslinked polymers and subsequent removal through partially dissolving or swelling the scaffold in organic solvents.[19] Other methods include designing easily-removeable support scaffolds that maintain limited contact with the printed part. With the development of multi-material printing systems, incorporation of physically crosslinked and dissolvable scaffolds into a system is now possible.[20]

In this work, vat photopolymerization AM enabled the creation of dissolvable parts where supramolecular interactions dictated monomer selection and facilitated the creation of water-swollen gels. The broad selection of functionalized monomers achieved a spectrum of mechanical properties, from elastomers to thermoplastics with a range of dissolution rates. Characterization of the photopolymerization process employed both differential scanning calorimetry and rheology, each coupled with a UV light source, which revealed a dependence of monomer functionality and water content. Tensile analysis revealed high elongation of each photopolymerized gel (up to 1200%), highlighting a strong dependence on water content and ionic interactions. Hysteresis experiments further confirmed the elastomeric properties of each system. Finally, vat photopolymerization of monomer solutions yielded well-defined printed parts, which retained water solubility. This report enables future study into dissolvable parts created through vat photopolymerization for fully soluble support scaffold applications.

2. Materials and methods

2.1. Materials

Trimethylammonium ethyl acrylate chloride solution (TMAEA, 80 wt% in water), 3-sulfopropyl acrylate potassium salt (SPAK), 2-acrylamido-2-methyl-1-propane sulfonic acid sodium salt (AASNa, 50 wt% in water), 2-acrylamido-2-methyl-1-propane sulfonic acid (AAS), *N*-vinyl pyrrolidone (NVP), and poly(ethylene glycol) methyl ether acrylate (PEGMEA_{480}) were purchased from Sigma-Aldrich. 2-Hydroxy-4′-(2-hydroxyethoxy)-2-methylpropiophenone (Irgacure 2959) and diphenyl(2,4,6-trimethylbenzoyl) phosphine oxide (TPO) were purchased from Sigma-Aldrich and dissolved in ethanol and acetone before use, respectively. 2,5-Bis(5-*tert*-butyl-benzoxazol-2-yl)thiophene (BBOT), a UV blocker, was purchased from Sigma-Aldrich and dissolved in NVP before use. All solvents were purchased from Spectrum, Inc. and used as received.

2.2. Analytical methods

Photocalorimetry (Photo-DSC) was performed on a TA Instruments Q2000 with an Omnicure S2000 photo-attachment with fiber optic cable. T-zero pans were loaded as either sample pans or reference pans and equilibrated at 25 °C. Following a 1 min isotherm, 8 mW cm^{-2} of 365 nm light was introduced to the pans. Following a 5 min irradiation, the light was turned off and the background heat from the light was noted. Integrations of the peaks with background correction afforded the heat of polymerization. To calculate percent conversion, the standard values for ΔH_{rxn} for the homopolymerization of acrylates and acrylamides (86 kJ mol^{-1})[21] and NVP (53.9 kJ mol^{-1})[22] were employed. The ΔH_{rxn} values obtained from photo-DSC were normalized based on the weight of each monomer used in the experiment. Photorheology of polymerized monomer occurred on a TA Instruments DHR-2 Discovery Rheometer with a photo-attachment and a 20 mm quartz bottom plate with 20 mm disposable upper geometry. Samples were equilibrated at 25 °C for 30 s to provide baselines for all samples. Samples were oscillated at 1 Hz, providing sampling rates relevant for the second timescale. Following 30 s, samples were irradiated at 8 mW cm^{-2} and the modulus was monitored. The crossover point was determined as the first instance that the storage modulus (G') exceeded loss modulus (G''). Tensile testing was performed on film-punched dogbones from photocured films with a crosshead motion of 500 mm min^{-1} and grip-to-grip separation of 26.25 mm on an Intron 5500R. Hysteresis testing was performed on film-punched dogbones from photocured films with a crosshead motion of 5 mm min^{-1}, 100% strain for five cycles with a grip-to-grip separation of 26.25 mm. The area under the curve was calculated using the trapezoid method[23] and the cycles were compared at $n = 5$ samples. Dynamic light scattering (DLS) was performed on a Malvern ZetaSizer at room temperature with a backscattering angle of 145° and a wavelength of 435 nm.

2.3. Film preparation

PEGMEA_{480}, TMAEA, and AASNa were used as received (0 wt%, 20 wt%, and 50 wt% water, respectively). AAS and SPAK were dissolved at 50 wt% water prior to use and NVP was used without further modification. 2 wt% photoinitiator in ethanol was added to monomer solutions to initiate the photopolymerization. Films were prepared by irradiation from a broad-band UV source at 8.5 mW cm^{-2} in an Ace Glass Incorporated photo-cabinet until they were free-standing. Typically, the film was exposed to UV light for 30 s per side to ensure full conversion. Films were used for subsequent analysis without further purification or extraction.

2.4. Dissolution testing

Sections of gel were placed in RO water at 1 mg mL^{-1} at 23 °C. The water was stirred rapidly with a magnetic stir bar and the time to full dissolution was noted. Data is presented as an average with a standard deviation of $n = 3$ samples.

2.5. 3D printing

TMAEA (20 wt% water) and combinations of TMAEA and NVP with 2 wt% TPO in acetone were added to a 50 mL vat of an Autodesk Ember® digital light processing (DLP) mask-projection stereolithography, bottom-up, 3D printer with a LED ultraviolet light source at 405 nm with an intensity of 20 mW cm^{-2}. Autodesk Print Studio design software imported 3D digital models as .stl files sent to the Autodesk Ember® for printing. The first layer was irradiated for 8 s to ensure adhesion to the stainless aluminum build platform. The next four layers were irradiated for 3 s, which incorporated intermediate layers to support the remaining layers. All subsequent model layers were each irradiated for 2 s. The set later thickness was 50 µm, which was controlled by linear actuation of the build stage in the vertical *z*-direction. Between each layer, the build stage was raised to allow fresh monomer solution onto the PDMS optical window and to recoat the part until the build was complete. Printed parts were gently detached from the build stage before analysis. Because of material incompatibilities with the Autodesk Ember®, printing of combinations containing *N*-vinyl pyrrolidone proceeded on a custom-build 3D printer. To begin the printing process, 1, 2, 2.5 and 3 wt% of TPO was added to a solution of TMAEA with 30 wt% NVP and 0.4 wt% BBOT. The formulations were irradiated with UV light for 5 s and the thickness of the irradiated film was measured. Beyond 2 wt% TPO, the thickness of the cured film reached convergence. The resin formulation with 2 wt% TPO was added to a vat and placed in the build area of a custom top-down mask-projection vat-photopolymerization machine. A build-stage with a glass substrate was inserted into the resin. A broad-spectrum UV light source (300–500 nm) irradiated the surface of the resin with an intensity of 1.96 mW cm^{-2} (measured at 365 nm). From the working curve,[24] the exposure time for curing 100 µm was estimated to be 5 s. Upon loading and slicing the .stl file with 100 µm layer thickness, the first layer was projected on the build stage. The stage was lowered by 100 µm and a fresh coat of resin was deposited in the build area. This process of projection and recoating continued till the complete part was fabricated. The parts were then removed from the build-stage, cleaned with ethanol, and patted dry with tissue. Printed parts were then irradiated in a UV post curing chamber for 10 min.

2.6. Shrinking study

3D printed cubes (1 × 1 × 1 cm) were placed on a porous substrate in a vacuum oven at 5 mbar and 60 °C from 0 to 24 h. Measurements were taken in the *x*, *y*, and *z* directions at 2, 4, 6, 8, 16, and 24 h where data is presented as an average of $n = 3$ samples.

2.7. Water-uptake/swelling study

3D printed cubes (1 × 1 × 1 cm) were dried for 24 h in a vacuum oven at 60 °C and 5 mbar for 24 h. The part was weighed and placed in 100 mL of water without agitation in order to encourage swelling and not dissolution. The weight of the part was measured at 2, 4, 6, 8, 16, and 24 h where the data is presented as an average of $n = 3$ samples. The surface of the parts were dried on the surface with tissue before weighing to prevent water accumulation on the surface from contributing to water-uptake measurements.

2.8. Statistical analysis

Statistical testing was performed using JMP software. An ANOVA test followed by a Tukey's HSD provided differences between treatment groups at 95% confidence.

2.9 Nomenclature

When referring to the copolymer systems of TMAEA and NVP, each sample is named "TMAEA-*co*-NVP" followed by the weight percent of NVP incorporation. As an example, a copolymer system with 2.5 wt% NVP is denoted as "TMAEA-*co*-NVP2.5".

3. Results and discussion

Traditional vat photopolymerization AM processes utilize chemical crosslinking to ensure part fidelity upon printing. However, this process generates a permanent chemical network with the inability to fully dissolve for support scaffold applications.[25] This work describes the identification of ionic monomers in water to afford a range of acrylate, acrylamide, and vinyl monomers suitable for the 3D printing of physically-crosslinked objects. Equivalent structures in acrylate *vs.* acrylamide (3-sulfopropyl acrylate potassium salt (SPAK)) *vs.* (2-acrylamido-2-methyl-1-propane sulfonic acid sodium salt (AASNa)) as well as ionic *vs.* acid forms (AASNa *vs.* 2-acrylamido-2-methyl-1-propane sulfonic acid (AAS)) provided a library of promising monomers to evaluate photopolymerized hydrogel properties and to aid future rational design (Scheme 1). TMAEA ultimately demonstrated mechanical properties most promising for vat photopolymerization, but to increase part strength and provide a range of water dissolution rates, *N*-vinyl pyrrolidone (NVP) was added as a comonomer.

TMAEA and *N*-vinyl pyrrolidone (NVP) copolymers provided the opportunity to observe a systematic change in mechanical properties and water dissolution rates based on NVP incorporation. The literature broadly describes free radical polymerization and reverse addition–fragmentation chain transfer polymerization of NVP copolymerized with acrylate and ammonium-containing monomers.[26–29] Roka *et al.* measured reactivity ratios of NVP and 2-(dimethylamino)ethyl methacrylate suggesting the formation of pseudo-diblock copolymers. They observed multiple glass transition temperatures of the copolymers where transitions near 180 °C were associated with the poly(*N*-vinyl pyrrolidone) (PVP) blocks.[27] The addition of NVP to copolymer systems with acrylates in the presence of

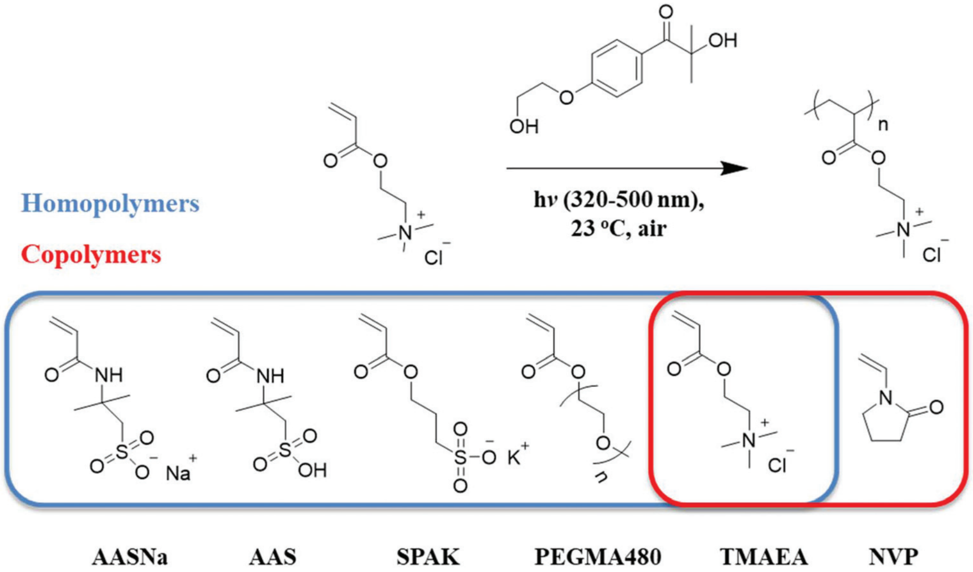

Scheme 1 Photopolymerization of various monomers in the presence of photoinitiator and UV irradiation to produce homopolymers and copolymers.

oxygen is also known to decrease inhibition during photopolymerization. It was hypothesized that molecular oxygen is quenched through photooxidation with the NVP amide bond or the formation of an excimer with the amide bond.[30] Thus, we propose that the copolymerization of TMAEA and NVP will provide higher strength materials and higher conversions compared to polyelectrolyte homopolymer systems. TMAEA proved the optimal candidate for vat photopolymerization based on photo-kinetics and mechanical properties from photo-polymerized films, which deemed this monomer as the most logical copolymer for the NVP-containing systems. This is a significant advantage for vat photopolymerization processes as most machines print in the presence of oxygen.

Photo-DSC and photorheology provided photo-kinetics of each system to aid in predicting specifications needed for vat photopolymerization. Photo-DSC generated heats of reaction (ΔH_{rxn}) as a function of irradiation time and allowed for estimations of polymerization rate and monomer conversion (Fig. 1A and B). TMAEA proved to evolve the most heat upon irradiation, potentially due to higher conversion percentages or a lower wt% water in the system. However, PEGMEA$_{480}$, which did not contain water, exhibited a broad peak and lower evolved heat of polymerization potentially due to lack of supramolecular interactions. Each of the acrylamide monomers (AAS and AASNa) experienced shorter times to peak heat flow compared to the equivalent acrylate (SPAK), suggesting a possible role of hydrogen bonding in the polymerization process or

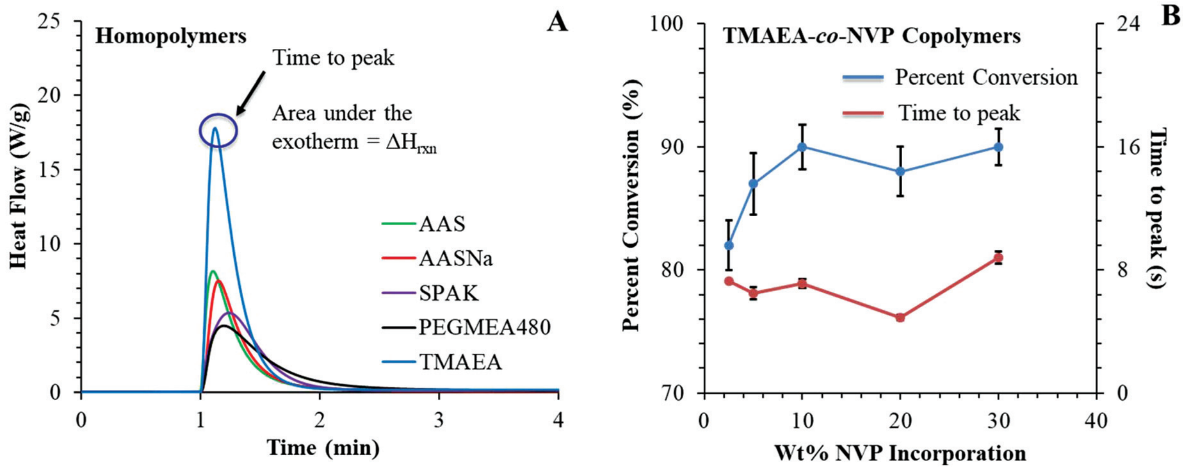

Fig. 1 (A) Heat flow as a function of time where UV light exposure began at 1 min for each homopolymer. The time to peak is denoted as the maxima in the trace and the area under the curve represents the ΔH_{rxn}. (B) Time to peak and ΔH_{rxn} as a function of wt% NVP incorporation.

acrylamide *vs.* acrylate reactivity.[31] Aqueous size exclusion chromatography of the photopolymerized systems attempted to measure molecular weights, but ionic aggregation prevented reproducible separation. The size of each of these aggregates and their shape potentially directed both the kinetics of polymerization and the properties of the free-standing film.[32,33] Further studies of the particular mechanism and the potential use of these monomers is currently underway.

Photo-DSC of TMAEA and NVP copolymerizations revealed an increase in ΔH_{rxn} with increasing NVP incorporation. The time to reach a maximum in heat flow was longer compared to the other polyelectrolyte systems, and a trend was not observed. Photo-DSC of neat NVP with either Irgacure 2959 or TPO revealed less than 12% conversion during the 5 min experiment. This observation suggested the formation of TMAEA-*co*-NVP copolymers rather than a blend of TMAEA and NVP homopolymers. Liska *et al.* observed a similar phenomenon where NVP reached the highest conversions with Irgacure 819 as a photoinitiator compared to multiple other photoinitiator systems. They hypothesized Irgacure 819 maintained the best solubility in NVP, which facilitated radical polymerization.[18]

After normalizing the ΔH_{rxn} values to the moles of monomer and using literature standards for 100% conversion of acrylates (86 kJ mol^{-1})[21] and NVP (53.9 kJ mol^{-1}),[22] the relative monomer percent conversions were calculated. TMAEA, AAS, AASNa, and SPAK exhibited conversions of 75, 35, 40, and 45%, respectively (Table S1†). TMAEA and SPAK, *i.e.* acrylate-containing monomers, exhibited statistically higher conversions compared to acrylamide-containing monomers (AAS and AASNa). The calculated conversions support the longer dissolution times for TMAEA and SPAK compared to AAS and AASNa. TMAEA had the highest conversion possibly due to ordering before polymerization. To further explore this hypothesis, complex viscosities for each monomer system dissolved in varying wt% water were studied, which suggests monomer ordering (Fig. S2†). TMAEA exhibited the largest complex viscosity in 20 wt% water (0.062 Pa s), which suggested an increase in ionic aggregation and ordering compared to the other samples.

TMAEA and NVP copolymer systems exhibited higher conversions (82–90%) compared to all homopolymers. As discussed previously, NVP is known to reduce termination in free radical polymerizations in the presence of oxygen.[30] As NVP incorporation increased, conversion increased, where statistical differences existed between TMAEA-*co*-NVP2.5 and TMAEA-*co*-NVP5, TMAEA-*co*-NVP10, TMAEA-*co*-NVP20, and TMAEA-*co*-NVP30. Most vat photopolymerization systems print in the presence of air through free radical polymerization where oxygen will terminate propagation. Adding a monomer that reduces termination provides advantages with part strength and fidelity. While unreacted monomer still exists in the discussed systems, ranging from an estimated 18–10% in the TMAEA-*co*-NVP copolymers, future use of oxygen scavenging components will potentially mitigate this problem.

Photorheology of monomers revealed a trend in plateau storage modulus (G_{N}°) as a function of monomer and water content in the homopolymer systems (Fig. 2A and B). G_{N}° values from photorheology provide a relative strength profile that will directly affect the vat photopolymerization process. TMAEA exhibited significantly increased G_{N}° following polymerization compared to all other monomers. Both the rate of polymerization and increased conversion likely led to a fast crossover time (2 s) and enhanced G_{N}°, lending itself as the prime candidate for vat photopolymerization. Despite its lower water content, PEGMEA$_{480}$ failed to reach the same G_{N}° as TMAEA, suggesting that the ionic interactions in TMAEA generated a more physically crosslinked film than non-charged PEGMEA$_{480}$. Furthermore, as SPAK, AAS, and AASNa each possessed 50 wt% water, direct comparisons between acrylate, acrylamide, and the role of ions was investigated. As confirmed from results of photo-DSC, SPAK exhibited a much slower rate of polymerization and thus a longer time to reach the G'–G'' crossover point (16 s) than either AAS (6 s) or AASNa (7 s). The

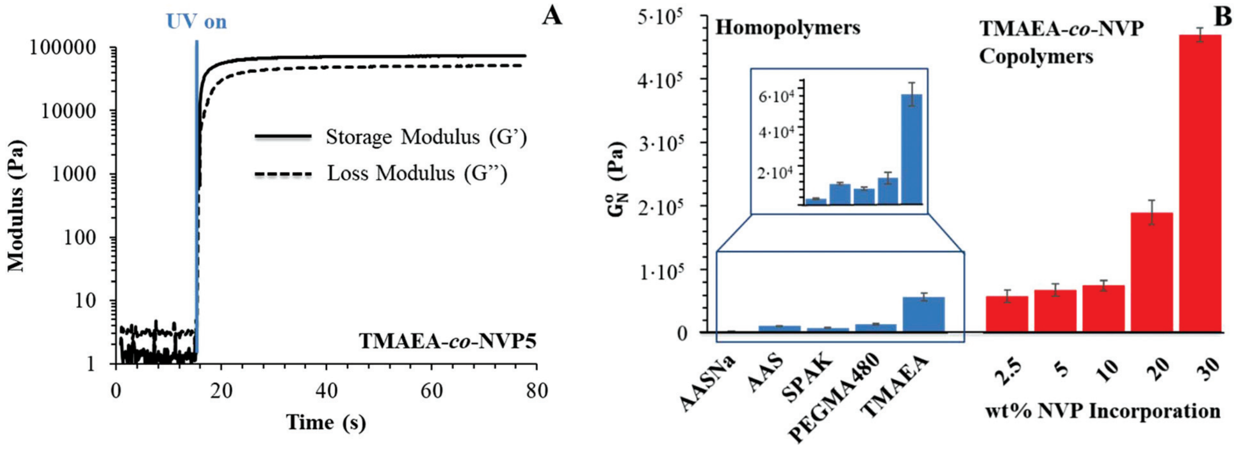

Fig. 2 (A) A representative photo-rheology trace where the sample is exposed to UV light after 15 s and the plateau storage modulus (G_{N}°) is denoted. (B) G_{N}° as a function of homopolymer composition and wt% NVP incorporation.

role of ion incorporation into monomers also afforded gels of varied modulus, as seen in the comparison between AAS and AASNa. When comparing AASNa to SPAK, the rate of polymerization potentially limits molecular weight growth after ~5 s of AASNa, while SPAK continues to polymerize over much longer time scales. The acid form of the acrylamide monomer generated moduli similar to PEGMEA$_{480}$ despite containing 50 wt% water.

Photorheology of TMAEA and NVP combinations revealed an apparent relationship between G_N° and NVP incorporation (Fig. 2B). The G_N° steadily increased from 0.058 MPa for TMAEA-*co*-NVP2.5 to 0.470 MPa for TMAEA-*co*-NVP30, which confirmed NVP increases the modulus of the hydrogels. Combinations containing above 30 wt% NVP resulted in inconsistent and non-reproducible measurements of mechanical properties, therefore the 30 wt% NVP incorporation was the highest included. These combinations contain fewer ionic interactions compared to neat TMAEA and other monomer systems discussed above. The increase in modulus is likely due to the high glass transition temperature of poly(vinyl pyrrolidone) (PVP), which ranges from 150–180 °C in the absence of water in the formation of pseudo-diblock copolymers.[27,29,34]

To further confirm the importance of electrostatic interactions in the resulting photopolymerized parts, two non-charged controls, 2-(dimethylamino)ethyl acrylate (DMAEA) and PEGMEA$_{480}$, were also tested. DMAEA is structurally equivalent to TMAEA besides the absence of an ammonium moiety. Photo-DSC and photo-rheology (Fig. S1A and S1B†) revealed low conversion values compared to the charged monomers and the absence of a crossover point in photo-rheology. The resulting product from photo-rheology was a viscous liquid, which is consistent when no crossover point is observed. PEGMEA$_{480}$ served as the second control because

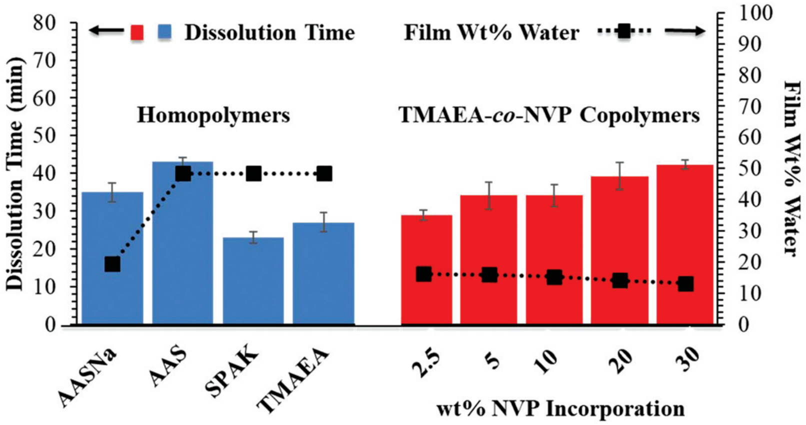

Fig. 3 Dissolution rate as a function of homopolymer composition and NVP incorporation with a magnetic stir bar at 1 mg mL^{-1} and 23 °C.

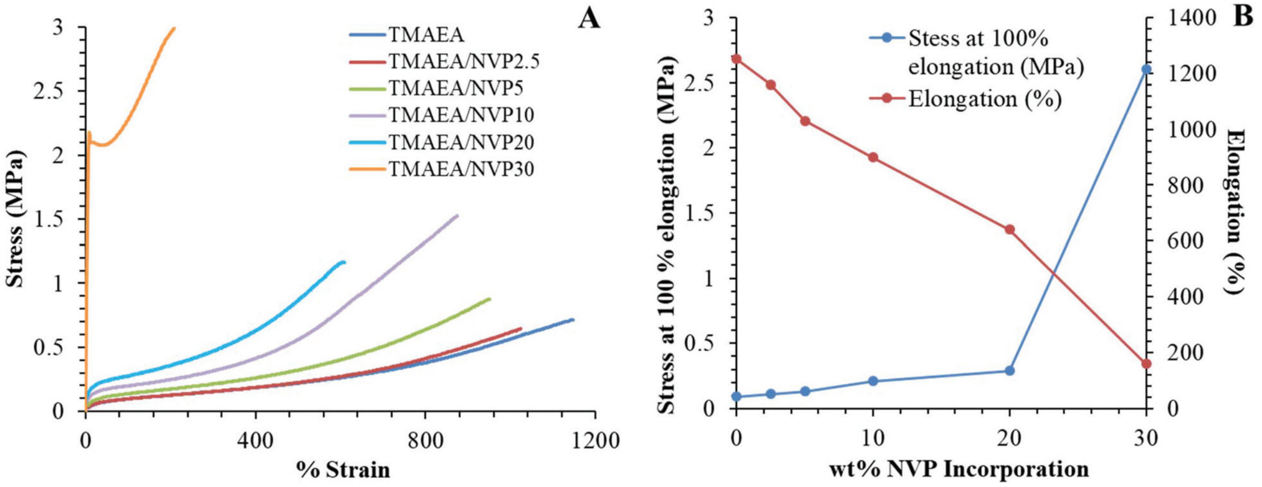

Fig. 4 (A) Stress *vs.* strain curves of photopolymerized unextracted films of TMAEA with 2.5 to 30 wt% NVP. (B) Stress at 100% elongation and strain at break as a function of wt% NVP incorporation.

this monomer was able to form solid parts after photopolymerizing, even though it does not have an equivalent structure to any of the charged monomers.

After measuring the photo-kinetics of the homopolymer and copolymers, controlled dissolution experiments determined water dissolution times of the photopolymerized films. Water dissolution studies also revealed an increase in dissolution time with increasing incorporation of NVP in TMAEA-*co*-NVP copolymers where statistical differences arose between TMAEA-*co*-NVP2.5, TMAEA-*co*-NVP20, and TMAEA-*co*-NVP30. This compositional range provided dissolution rates ranging from 27 to 41 min, which demonstrated the potential to 3D print fully dissolvable parts using vat photopolymerization. Because vat photopolymerization usually employs covalent crosslinks that render the final part insoluble, this system has the potential to serve as a dissolvable support scaffold.

The role of physical crosslinks in the dissolution of photopolymerized parts will be an essential part of soluble support scaffold applications. Exposure to excess water resulted in the dissociation of the charges and their counterions, which facilitated the breaking up of electrostatic aggregates and full dissolution. As noted in Fig. 3, monomer type, acrylamides *vs.* acrylates (SPAK, AASNa), dictated the time to full dissolution, while wt% water in the films did not influence the rates. Statistical differences arose between all acrylate- and acrylamide-containing systems, but a trend was not observed between different supramolecular interactions (ionic *vs.* acid forms). This suggested a higher degree of polymerization resulting from acrylate- *vs.* acrylamide-containing systems where increased molecular weight presumably increased dissolution time. Photo-DSC explored this hypothesis further. Interestingly, PEGMEA_{480} failed to dissolve in water after more than 24 h under the described conditions.[35]

As described in Fig. 3, each film or printed object contained varying amounts of water, leading to hydrogels. The subsequent mechanical testing was performed using unextracted, water-swollen gels where the presence of water greatly aided to the elastic behavior. After elimination of water upon heating at 80 °C under high vacuum for 24 h, the films or printed parts became rigid and brittle. The parts were also very hydroscopic, and exposure to atmospheric conditions for only minutes resulted in sticky surfaces.

Tensile tests revealed strength, elongation, and hysteresis for each system. Tensile experiments of photopolymerized TMAEA-*co*-NVP films revealed a systematic increase in stress at 100% elongation and decrease of strain at break when increasing NVP content, depicted in Fig. 4A and B. The photopolymerized film of neat TMAEA experienced the largest strain at break possibly due to the highest level of ionic interactions as physical crosslinks and the most water content acting as a plasticizer. As the incorporation of NVP increased from 2.5 to 30 wt%, the material transformed from a typical thermoplastic elastomer (TPE) to an engineering plastic based on the tensile analysis. Samples containing 2.5 to 20 wt% NVP did not experience a distinct linear region at the beginning of the experiment or demonstrate a measurable yield stress, which is consistent with elastomeric materials. TMAEA-*co*-NVP30 contained a distinct linear region with a yield stress, indicating toughness owing to the large wt% of NVP incorporation. Fig. 4B emphasizes the large increase in stress at 100% elongation from TMAEA-*co*-NVP20 to TMAEA-*co*-NVP30, which possibly arose from macrophase separation of the copolymers present in TMAEA-*co*-NVP30, depicted visually in Fig. 5.[36] Fig. 5A, B, and C depict photopolymerized films of TMAEA, TMAEA-*co*-NVP10, and TMAEA-*co*-NVP30, respectively. TMAEA appeared optically clear while increasing NVP incorporation resulted in increasing opaqueness. The tensile data from samples PEGMEA480, AAS, AASNa, and SPAK is included in the supplemental section (Table S3†) and follows similar trends demonstrated from photorheology.

Hysteresis experiments at 100% elongation over five cycles confirmed the elastomeric properties of TMAEA-*co*-NVP combinations. Fig. 6A depicts the hysteresis profile of TMAEA photopolymerized films. This data revealed low amounts of hysteresis after five cycles (9–14%), which suggested the physical ionic crosslinks and water plasticization resisted permanent deformation. Fig. 6B depicts TMAEA-*co*-NVP10 hysteresis profile, which begins to show residual strain and permanent deformation after each cycle. The hysteresis profile of TMAEA-*co*-NVP30, depicted in Fig. 6C, reveals the most hysteresis and most residual strain compared to the previous two samples. After cycle 1, TMAEA-*co*-NVP30 experiences an average of 28% residual strain and does not recover after each cycle. While physical ionic crosslinks and water-plasticization provide some elastic properties, the data suggests the PVP pseudo-blocks experience permanent deformation.[37]

Vat photopolymerization of TMAEA with 2 wt% TPO revealed the fabrication of fine features upon rapid printing. As the printing proceeded, residual TMAEA, near 25%, resided

Fig. 5 (A) Photopolymerized films of TMAEA, (B) TMAEA-*co*-NVP10 copolymer, and (C) TMAEA-*co*-NVP30 copolymer.

within the part interior and was trapped within the structure based on monomer conversion values measured using photo-DSC. Other observations included overcure due to the rapid polymerization of TMAEA monomer likely played a role in part fidelity. As shown in Fig. 7A, the top crenellations in the rook design maintained fine feature resolution characteristic of vat photopolymerization. Due to the solubility of printed parts, uncured monomer remained within the printed part, despite drying steps, prior to scanning electron microscopy (SEM). When examined further using SEM (Fig. 7B), the crenellations exhibited a surface roughness characteristic of the layer thickness because of light penetration within each layer. Despite this characteristic surface roughness, distinct layers did not develop, suggesting strong interlayer interactions and a blending of layers during the print process. The physical properties of printed parts rival those seen in bulk gels, suggesting a lack of anisotropy characteristic in traditional 3D printed parts.

A top-down vat-photopolymerization system enabled the fabrication of complex lattice structures with pillar widths as small as 500 μm, depicted in Fig. 7C. TMAEA and NVP system exhibit high G_N°, which facilitated the printing of self-supporting geometries. Printing with 2 wt% TPO without the addition of photo-blocker resulted in overcure and structural imperfections within the lattice. With the addition of 0.4 wt% BBOT, the polymerized area remained within the area exposed to UV light, creating a lattice structure with high accuracy compared to the programmed CAD design.

Vat polymerization of 1 × 1 × 1 cm cubes of each TMAEA and TMAEA-*co*-NVP30 provided well-defined 3D parts for shrinking and swelling studies. Fig. 8A depicts water-uptake of TMAEA and TMAEA-*co*-NVP30 printed parts where both exceeded 5000% uptake. TMAEA reached 9000% water-uptake after 24 h owing to its higher ionic content compared to TMAEA-*co*-NVP30.[38,39] TMAEA-*co*-NVP30 also exhibited a larger range of standard deviations because some samples did not maintain a uniform shape and partially dissolved. Fig. 8B depicts % shrinkage of each sample in the *x*, *y*, and *z* directions revealing an average of 17 and 13% isotropic shrinkage of TMAEA and TMAEA-*co*-NVP30, respectively. The larger % shrinkage in the neat TMAEA sample arose from the larger wt% water content of the hydrogel before drying, 20 wt%, compared to TMAEA-*co*-NVP30, 13.3 wt%. The varying shrinkage rates of each sample and in each direction may have resulted from non-uniform heating in the vacuum oven or variation in the surface exposure to the vacuum, as one side was placed on a porous surface.

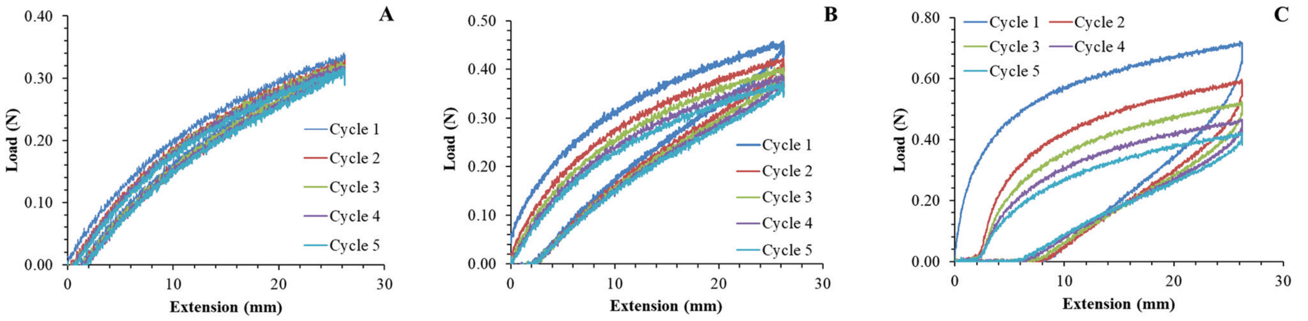

Fig. 6 Hysteresis experiments at 100% elongation for five cycles of (A) TMAEA, (B) TMAEA-*co*-NVP10, and (C) TMAEA-*co*-NVP30 photopolymerized films.

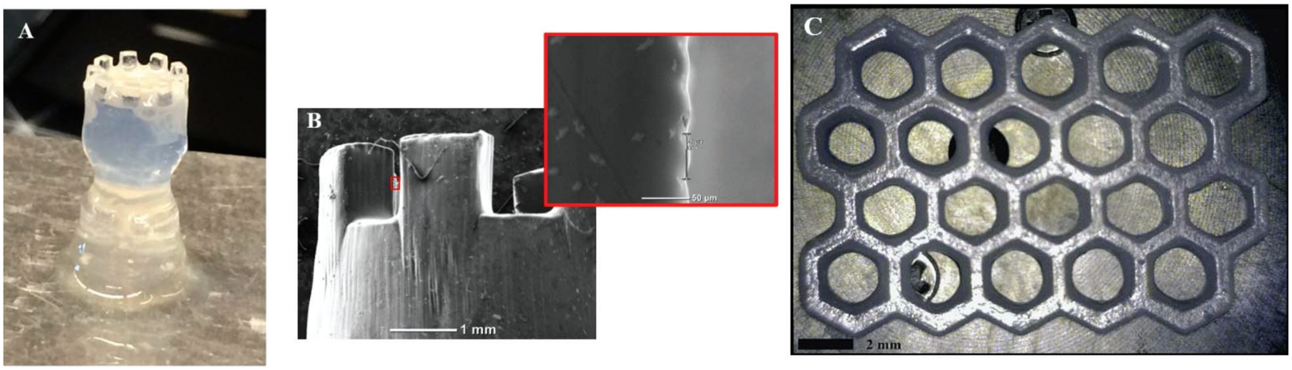

Fig. 7 (A) Vat photopolymerization of a rook with TMAEA using an Autodesk Ember. (B) SEM imaging reveals distinct crenellations and characteristic surface roughness relative to layer thickness. (C) Top-down vat photopolymerization with TMAEA-*co*-NVP30 fabricated a complex lattice structure with pillar widths as small as 500 μm.

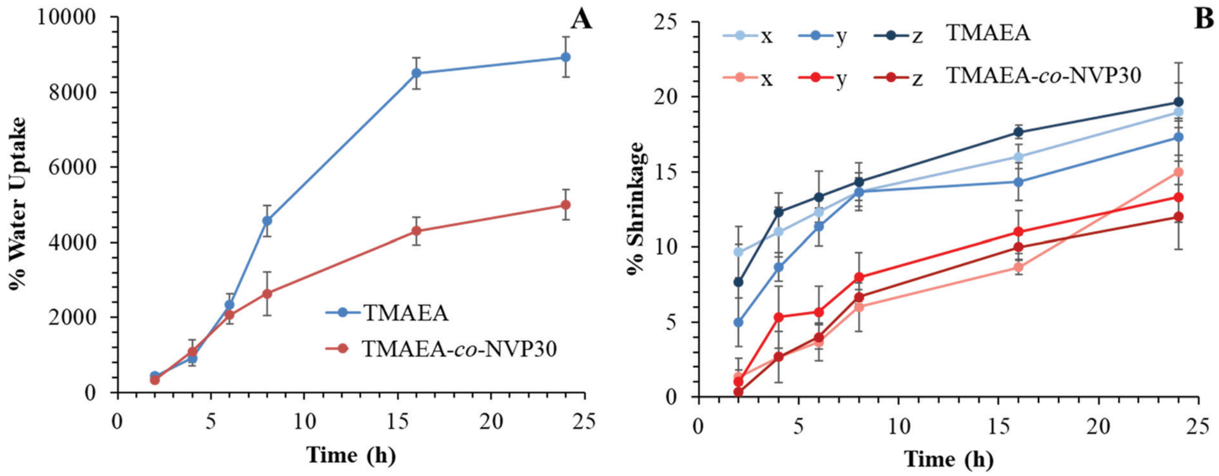

Fig. 8 (A) Percent water uptake for TMAEA and TMAEA-*co*-NVP30 based on mass over 24 h. (B) Shrinking studies of TMAEA and TMAEA-*co*-NVP30 under high vacuum at 40 °C for 24 h.

4. Conclusion

Fully-soluble 3D printed parts employing ionic interactions resulted from vat photopolymerization additive manufacturing processes. These fully-soluble, 3D printed parts represent a new class of materials for high resolution, vat photopolymerization and this concept has the potential to enable soluble support scaffolds. This report details the characterization of water-soluble gels created through photopolymerization. A wide range of monomers afforded the development of a broad spectrum of gel properties based on supramolecular interactions. TMAEA and NVP combinations demonstrated tunable mechanical properties from TPEs to engineering plastics. Furthermore, preliminary investigation using a vat photopolymerization additive manufacturing process produced parts with well-defined features and the absence of defined layers, paving the way for future work to examine the limits of resolution and properties afforded by this process.

Conflicts of interest

There are no conflicts to declare.

Acknowledgements

The authors would like to thank Dr Charles Carfagna for analytical support.

References

1 U. G. Wegst, H. Bai, E. Saiz, A. P. Tomsia and R. O. Ritchie, Bioinspired structural materials, *Nat. Mater.*, 2015, **14**(1), 23–36.

2 B. G. Compton and J. A. Lewis, 3D-printing of lightweight cellular composites, *Adv. Mater.*, 2014, **26**(34), 5930–5935.

3 H. N. Chia and B. M. Wu, Recent advances in 3D printing of biomaterials, *J. Biol. Eng.*, 2015, **9**(1), 4.

4 B. C. Gross, J. L. Erkal, S. Y. Lockwood, C. Chen and D. M. Spence, *Evaluation of 3D printing and its potential impact on biotechnology and the chemical sciences*, ACS Publications, 2014.

5 W. Gao, Y. Zhang, D. Ramanujan, K. Ramani, Y. Chen, C. B. Williams and P. D. Zavattieri, The status, challenges, and future of additive manufacturing in engineering, *Computer Aided Design*, 2015, **69**, 65–89.

6 A. R. Schultz, P. M. Lambert, N. A. Chartrain, D. M. Ruohoniemi, Z. Zhang, C. Jangu and T. E. Long, 3D Printing Phosphonium Ionic Liquid Networks with Mask Projection Microstereolithography, *ACS Macro Lett.*, 2014, **3**(11), 1205–1209.

7 J. M. Sirrine, A. M. Pekkanen, A. M. Nelson, N. A. Chartrain, C. B. Williams and T. E. Long, 3D-printable biodegradable polyester tissue scaffolds for cell adhesion, *Aust. J. Chem.*, 2015, **68**(9), 1409–1414.

8 C. M. Spadaccini, G. Farquar, T. Weisgraber, S. Gemberling, N. Fang, J. Xu, M. Alonso and H. Lee, High resolution projection micro stereolithography system and method, *US Pat.*, US949269B2, 2016.

9 J. M. Sirrine, V. Meenakshisundaram, N. G. Moon, P. J. Scott, R. J. Mondschein, T. F. Weiseman and T. E. Long, Functional siloxanes with photo-activated, simultaneous chain extension and crosslinking for lithography-based 3D printing, *Polymer*, 2018, **152**, 25–34.

10 J. W. Stansbury and M. J. Idacavage, 3D printing with polymers: Challenges among expanding options and opportunities, *Dent. Mater.*, 2016, **32**(1), 54–64.

11 W. Lu, X. Le, J. Zhang, Y. Huang and T. Chen, Supramolecular shape memory hydrogels: a new bridge between stimuli-responsive polymers and supramolecular chemistry, *Chem. Soc. Rev.*, 2017, **46**(5), 1284–1294.

12 M. J. Webber, E. A. Appel, E. Meijer and R. Langer, Supramolecular biomaterials, *Nat. Mater.*, 2016, **15**(1), 13–26.

13 M. Akar, O. Sirkecioglu and N. Bicak, Synthesis of methacrylate pendant polyelectrolyte as water-soluble multifunctional cross-linker, *Eur. Polym. J.*, 2017, **97**, 418–422.

14 K. Zhang, M. Aiba, G. B. Fahs, A. G. Hudson, W. D. Chiang, R. B. Moore and T. E. Long, Nucleobase-functionalized acrylic ABA triblock copolymers and supramolecular blends, *Polym. Chem.*, 2015, **6**(13), 2434–2444.

15 K. Zhang, M. Chen, K. J. Drummey, S. J. Talley, L. J. Anderson, R. B. Moore and T. E. Long, Ureido cytosine and cytosine-containing acrylic copolymers, *Polym. Chem.*, 2016, **7**(43), 6671–6681.

16 E. M. Wilts, J. Herzberger and T. E. Long, Addressing water scarcity: cationic polyelectrolytes in water treatment and purification, *Polym. Int.*, 2018, **67**, 799–814.

17 C. B. Highley, C. B. Rodell and J. A. Burdick, Direct 3D printing of shear-thinning hydrogels into self-healing hydrogels, *Adv. Mater.*, 2015, **27**(34), 5075–5079.

18 R. Liska, F. Schwager, C. Maier, R. Cano-Vives and J. Stampfl, Water-soluble photopolymers for rapid prototyping of cellular materials, *J. Appl. Polym. Sci.*, 2005, **97**(6), 2286–2298.

19 C. Xia and N. Fang, Fully three-dimensional microfabrication with a grayscale polymeric self-sacrificial structure, *J. Micromech. Microeng.*, 2009, **19**(11), 115029.

20 S. Ready, G. Whiting and T. N. Ng, in Multi-material 3D printing, NIP & Digital Fabrication Conference, Society for Imaging Science and Technology, 2014, pp. 120–123.

21 E. Andrzejewska and M. Andrzejewski, Polymerization kinetics of photocurable acrylic resins, *J. Polym. Sci., Part A: Polym. Chem.*, 1998, **36**(4), 665–673.

22 BASF Published value.

23 B. Rljdf, *Numerical Analysis*, Brooks/Cole, 7th edn, 2000.

24 P. F. Jacobs, *Rapid prototyping & manufacturing: fundamentals of stereolithography*, Society of Manufacturing Engineers, 1992.

25 J. Wang, A. Goyanes, S. Gaisford and A. W. Basit, Stereolithographic (SLA) 3D printing of oral modified-release dosage forms, *Int. J. Pharm.*, 2016, **503**(1), 207–212.

26 A. Guinaudeau, O. Coutelier, A. l. Sandeau, S. p. Mazières, H. D. Nguyen Thi, V. Le Drogo and M. Destarac, Facile access to poly (N-vinylpyrrolidone)-based double hydrophilic block copolymers by aqueous ambient RAFT/MADIX polymerization, *Macromolecules*, 2013, **47**(1), 41–50.

27 N. Roka, O. Kokkorogianni and M. Pitsikalis, Statistical copolymers of N-vinylpyrrolidone and 2-(dimethylamino) ethyl methacrylate via RAFT: Monomer reactivity ratios, thermal properties, and kinetics of thermal decomposition, *J. Polym. Sci., Part A: Polym. Chem.*, 2017, **55**(22), 3776–3787.

28 A. Singhal and S. Chauhan, Free Radical Copolymerization of Acrylamide and N-Vinylpyrrolidone Catalyzed by Iron(III) porphyrins in the Presence of Ionic Liquids, *Org. Prep. Proced. Int.*, 2018, **50**(3), 359–371.

29 N. Gatica, N. Fernández, A. Opazo, S. Alegría, L. Gargallo and D. Radic, Synthesis and characterization of functionalized vinyl copolymers. Electronegativity and comonomer reactivity in radical copolymerization, *Polym. Int.*, 2003, **52**(8), 1280–1286.

30 T. J. White, W. B. Liechty and C. A. Guymon, The influence of N-vinyl pyrrolidone on polymerization kinetics and thermo-mechanical properties of crosslinked acrylate polymers, *J. Polym. Sci., Part A: Polym. Chem.*, 2007, **45**(17), 4062–4073.

31 D. J. Lloyd, V. Nikolaou, J. Collins, C. Waldron, A. Anastasaki, S. P. Bassett and K. Kempe, Controlled aqueous polymerization of acrylamides and acrylates and "in situ" depolymerization in the presence of dissolved CO 2, *Chem. Commun.*, 2016, **52**(39), 6533–6536.

32 S. A. M. Noor, J. Sun, D. R. MacFarlane, M. Armand, D. Gunzelmann and M. Forsyth, Decoupled ion conduction in poly (2-acrylamido-2-methyl-1-propane-sulfonic acid) homopolymers, *J. Mater. Chem. A*, 2014, **2**(42), 17934–17943.

33 M. M. Abdullah, A. A. AlQuraishi, H. A. Allohedan, A. O. AlMansour and A. M. Atta, Synthesis of novel water soluble poly (ionic liquids) based on quaternary ammonium acrylamidomethyl propane sulfonate for enhanced oil recovery, *J. Mol. Liq.*, 2017, **233**, 508–516.

34 P. Molyneux, *Water-Soluble Synthetic Polymers: Volume I: Properties and Behavior*, CRC press, 2018.

35 W. Wang, R. Liu, Z. Li, C. Meng, Q. Wu and F. Zhu, Synthesis and Self-Assembly of New Double-Crystalline Amphiphilic Polyethylene-block-Poly [oligo (ethylene glycol) Methyl Ether Methacrylate] Coil-Brush Diblock Copolymer, *Macromol. Chem. Phys.*, 2010, **211**(13), 1452–1459.

36 L. Leibler, Theory of microphase separation in block copolymers, *Macromolecules*, 1980, **13**(6), 1602–1617.

37 F. Luo, T. L. Sun, T. Nakajima, T. Kurokawa, Y. Zhao, K. Sato and J. P. Gong, Oppositely Charged Polyelectrolytes Form Tough, Self-Healing, and Rebuildable Hydrogels, *Adv. Mater.*, 2015, **27**(17), 2722–2727.

38 M. Rubinstein, R. H. Colby, A. V. Dobrynin and J.-F. Joanny, Elastic modulus and equilibrium swelling of polyelectrolyte gels, *Macromolecules*, 1996, **29**(1), 398–406.

39 V. S. Meka, M. K. Sing, M. R. Pichika, S. R. Nali, V. R. Kolapalli and P. Kesharwani, A comprehensive review on polyelectrolyte complexes, *Drug Discovery Today*, 2017, **22**, 1697–1706.